



Highly stable Pd/HNb3O8-based flexible humidity sensor for perdurable wireless wearable applications

Journal:	<i>Nanoscale Horizons</i>
Manuscript ID	NH-COM-10-2020-000594.R2
Article Type:	Communication
Date Submitted by the Author:	21-Dec-2020
Complete List of Authors:	<p>Lu, Yuyao; Osaka Prefecture University Xu, Kaichen; Osaka Prefecture University, Electrical and Computer Engineering Yang, Min-Quan; Fujian Normal University, College of Environmental Science and Engineering Tang, Shin-Yi; National Tsing Hua University Yang, Tzu-Yi; National Tsing Hua University, Department of Materials Science and Engineering Fujita, Yusuke; Osaka Prefecture University, Department of Physics and Electronics Honda, Satoko; Osaka Prefecture University, Department of Physics and Electronics Arie, Takayuki; Osaka Prefecture University, Department of Physics and Electronics Akita, Seiji; Osaka Prefecture University, Department of Physics and Electronics Chueh, Yu-Lun; National Tsinghua Univeristy, Materials Science and Engineering Takei, Kuniharu; Osaka Prefecture University, Department of Physics and Electronics</p>

Highly stable Pd/HNb₃O₈-based flexible humidity sensor for perdurable wireless wearable applications

Yuyao Lu^a, Kaichen Xu^a, Min-Quan Yang^b, Shin-Yi Tang^c, Tzu-Yi Yang^c, Yusuke Fujita^a, Satoko Honda^a, Takayuki Arie^a, Seiji Akita^a, Yu-Lun Chueh^c, and Kuniharu Takei^{*a,d}

New concepts

Flexible functional nanomaterials-based humidity sensors face challenges in achieving long-time perdurable performance, especially at high humidity range (>70% RH), limiting their practical applications in wearable healthcare and non-contact human-machine interfaces. Although various strategies have been applied to optimize the sensitivity and response/recovery time of humidity sensors, the stability and reproducibility still remain unresolved. To address the challenges, we propose a highly stable flexible humidity sensor based on Pd-modified HNb₃O₈ nanosheets. This new strategy utilized a photo-deposition method to generate abundant H atoms on the Pd surface, which plays a significant role in regulating the concentration of hydroniums by reducing part of them to water molecules, therefore enhancing the stability of Pd/HNb₃O₈ humidity sensor. Under over 100 h of cycle test, even at 90% RH, the proposed Pd/HNb₃O₈ humidity sensor presents almost no performance degradation, indicating a commendable sensing performance for perdurable applications. Furthermore, the respiration monitoring and real-time finger moisture detection indicate that this humidity sensor is highly reliable for long-time applications.

ARTICLE

Highly stable Pd/HNb₃O₈-based flexible humidity sensor for perdurable wireless wearable applications

Received 00th January 20xx,
Accepted 00th January 20xx

DOI: 10.1039/x0xx00000x

Yuyao Lu^a, Kaichen Xu^{a(1)}, Min-Quan Yang^b, Shin-Yi Tang^c, Tzu-Yi Yang^c, Yusuke Fujita^a, Satoko Honda^a, Takayuki Aric^a, Seiji Akita^a, Yu-Lun Chueh^c, and Kuniharu Takei^{*a,d}

Real-time, daily health monitoring can provide large amounts of patient data, which may greatly improve the likelihood of diagnosing health conditions in the early stage. One potential sensor is a flexible humidity sensor to monitor moisture and humidity information such as dehydration. However, achieving a durable functional nanomaterials-based flexible humidity sensor remains a challenge due to partial desorption of water molecules during the recovery process, especially at high humidities. In this work, we demonstrate a highly stable resistive-type Pd/HNb₃O₈ humidity sensor, which exhibits a perdurable performance for over 100 h of cycle tests under a 90% relative humidity (RH) without significant performance degradation. One notable advantage of the Pd/HNb₃O₈ humidity sensor is its ability to regulate hydroniums due to the strong reducibility of H atoms dissociated on the Pd surface. This feature realizes a high stability even at a high humidity (99.9% RH). Using this superior performance, the Pd/HNb₃O₈ humidity sensor realizes wireless monitoring of the changes in the fingertip humidity of an adult under different physiological states, demonstrating a facile and reliable path for dehydration diagnosis.

New concepts

Flexible functional nanomaterials-based humidity sensors face challenges in achieving long-time perdurable performance, especially at high humidity range (>70% RH), limiting their practical applications in wearable healthcare and non-contact human-machine interfaces. Although various strategies have been applied to optimize the sensitivity and response/recovery time of humidity sensors, the stability and reproducibility still remain unresolved. To address the challenges, we propose a highly stable flexible humidity sensor based on Pd-modified HNb₃O₈ nanosheets. This new strategy utilized a photo-deposition method to generate abundant H atoms on the Pd surface, which plays a significant role in regulating the concentration of hydroniums by reducing part of them to water molecules, therefore enhancing the stability of Pd/HNb₃O₈ humidity sensor. Under over 100 h of cycle test, even at 90% RH, the proposed Pd/HNb₃O₈ humidity sensor presents almost no performance degradation, indicating a commendable sensing performance for perdurable

applications. Furthermore, the respiration monitoring and real-time finger moisture detection indicate that this humidity sensor is highly reliable for long-time applications.

Introduction

The technology for flexible sensors has advanced greatly in the past decade.¹⁻³ Among diverse types of sensors, flexible humidity sensors have received much attention as a non-invasive disease diagnosis,⁴ wearable human respiration monitoring,⁵⁻⁸ and intelligent agriculture that can be incorporated in daily life.⁹⁻¹¹ They can be grouped into different types according to the sensing mechanism: resistive,^{8, 9, 12} capacitive,¹³⁻¹⁵ surface acoustic wave (SAW),¹⁶ and quartz crystal microbalance (QCM) types.¹⁷ Among these, resistive-type humidity sensors have been studied widely due to its facile fabrication, low cost, and commendable performance. This type of humidity sensor displays a signal of resistance change due to the interaction with water molecules. To date, various nanomaterials have been investigated as resistive humidity sensors, such as graphene oxide,¹⁸⁻²¹ carbon nanotubes (CNTs),^{22, 23} MoS₂,²⁴⁻²⁶ VS₂,¹² and WS₂,²⁷ owing to their highly exposed surface areas, abundant hydrophilic sites, and effective surface modification.

One limitation of most reported flexible humidity sensors is they are restricted to short-time cycle measurements primarily due to the partial desorption of water molecules from the device surface during the recovery process. Hence, long-time practical applications are limited. For example, Feng *et al.* demonstrated a highly sensitive ultrathin VS₂ nanosheets-based humidity sensor with a wide detection range of relative humidity (RH) from 0 to 100%, but the cycling tests were hundreds of seconds.¹² This reveals that the sensitivity and

^a Department of Physics and Electronics, Osaka Prefecture University Sakai, Osaka 599-8531, Japan.

^b Fujian Key Laboratory of Pollution Control & Resource Reuse, College of Environmental Science and Engineering, Fujian Normal University Fuzhou, Fujian 350007, China.

^c Department of Materials Science and Engineering, National Tsing-Hua University Hsinchu 30013, Taiwan, R.O.C.

^d JST PRESTO, Kawaguchi, Saitama 332-0012, Japan.

Email: takei@pe.osakafu-u.ac.jp

⁽¹⁾ Present address: State Key Laboratory of Fluid Power and Mechatronic Systems, School of Mechanical Engineering, Zhejiang University, Hangzhou 310027, China.

† Electronic Supplementary Information (ESI) available.

See DOI: 10.1039/x0xx00000x

stability of the present humidity sensors are still insufficient for long-time applications. Tremendous efforts have been devoted to optimizing the performance of humidity flexible sensors. Wu *et al.* introduced a porous and hydrophobic liquid crystal polymer substrate to reduce the response and recovery times of a graphene oxide-based humidity sensor.²⁰ Additionally, Li *et al.* designed a Ti₃C₂-derived TiO₂ nanowires-based humidity sensor with a sensitivity much higher than that of a pristine TiO₂-based humidity sensor.¹⁴ Although optimization improves the sensitivity and response time, humidity sensors show transitory stability in real-time cycle tests. To enhance the stability of humidity sensors, further material development, device structure, and applications are still required.

In this study, we demonstrate a flexible Pd/HNb₃O₈ humidity sensor with a high stability during cycle tests longer than 100 h. With the deposition of Pd on pristine HNb₃O₈ nanosheets, H₂ generated in the redox reaction is split into hydrogen atoms on the Pd surface due to its strong dissociation ability of H₂.^{28, 29} Previous studies have used Pd/HNb₃O₈ nanosheets as catalysts for energy conversion and storage fields due to their high surface area and suitable bandgap for electron transfer. However, their response to humidity has yet to be reported. Continuous measurements with the humidity sensor under a high RH confirm that the highly reductive H atoms on a Pd surface easily reduce the excess hydroniums to water molecules. Consequently, the

stability of this device is maintained. This critical change improves the device performance via a chemical modification method. Such an optimization method not only maintains a good sensitivity of the HNb₃O₈ humidity sensor, but also guarantees durability in future applications. Due to the reliable sensing performance of the Pd/HNb₃O₈ humidity sensor, we monitored the real-time finger moisture of an adult under different physiological states while exercising. This measurement successfully captured the perspiration condition of one subject by monitoring the change in skin moisture as a signal of a physiological response. The proposed surface modification method provides a new guide to increase the stability and reproducibility of two-dimensional nanomaterials-based humidity sensors.

Results and discussion

Stacked Pd/HNb₃O₈ nanosheets were synthesized via a photo-deposition process.²⁹ A small quantity of Pd particles is deposited on the HNb₃O₈ nanosheets surface by a photoredox reaction under UV light irradiation (Figure 1a). The Pd/HNb₃O₈ humidity sensor is composed of intersecting laser-induced graphene (LIG) electrodes and a stacked Pd/HNb₃O₈ nanosheets layer (Figure 1b and S1, ESI†). Scanning electron microscope (SEM) images indicate a slightly wrinkled surface morphology and lamellar structure of stacked

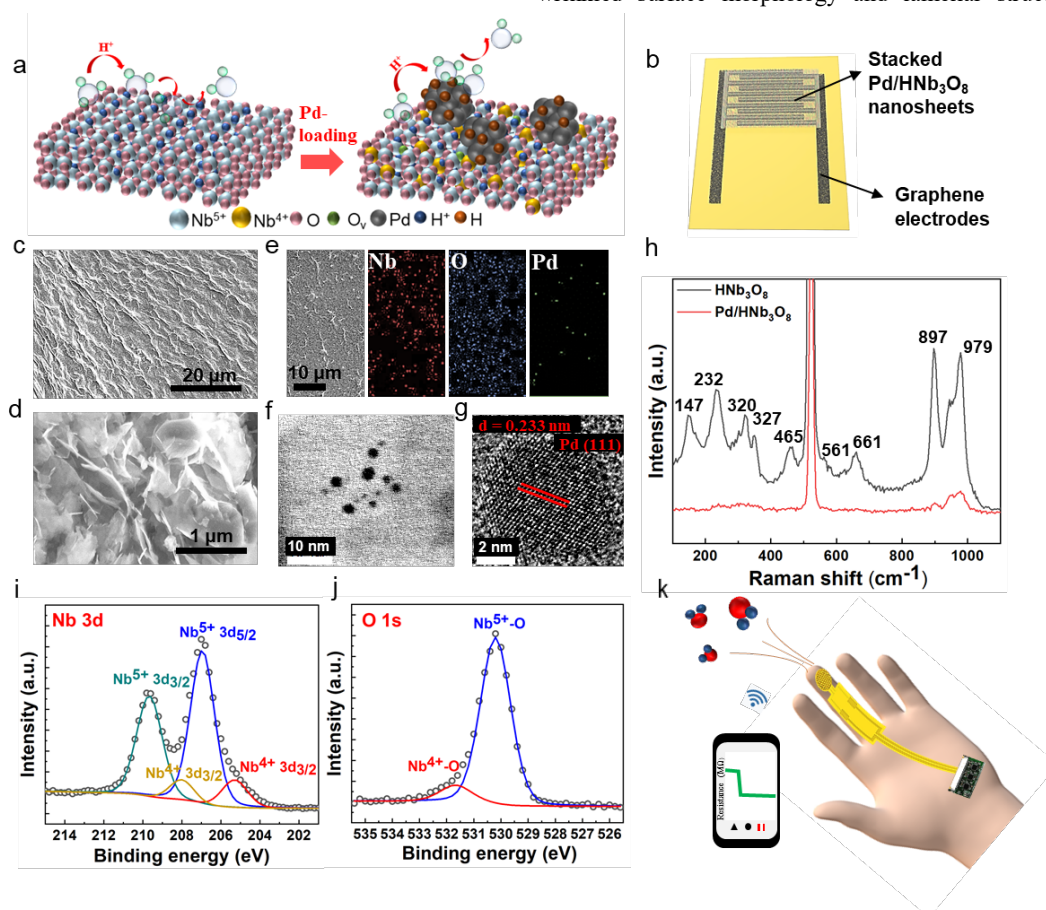


Figure 1. Schematics of (a) HNb₃O₈ and H-atom-enriched Pd-doped HNb₃O₈ and (b) the Pd/HNb₃O₈ humidity sensor. (c)–(d) Surface morphology and (e) SEM-EDX images for the Nb, O, and Pd distributions of the Pd/HNb₃O₈ nanosheets. (f) TEM image of Pd nanoparticles on ultrathin HNb₃O₈ nanosheets. (g) HRTEM analysis of the Pd nanoparticles. (h) Raman spectrum of pristine HNb₃O₈ and Pd/HNb₃O₈. XPS spectra of (i) Nb 3d and (j) O 1s for Pd/HNb₃O₈. (k) Schematic of a wireless finger moisture application.

Pd/HNb₃O₈ nanosheets (Figure 1c–d). These observations are similar to those of pristine HNb₃O₈ nanosheets (Figure S2–S3, ESI†). The energy-dispersive X-ray spectroscopy (EDX) results show the distribution of different elements in ultrathin Pd/HNb₃O₈ nanosheets and reveal well dispersed Pd nanoparticles throughout the nanosheets surface (Figure 1e). Transmission electron microscopy (TEM) was employed to survey the Pd nanoparticles distributed on the ultrathin nanosheets surface (Figure 1f–g), indicating a lattice constant of 0.233 nm. This agrees well with the interplanar distance between the lattice planes of metallic Pd (111).³⁰ Compared to pristine HNb₃O₈ nanosheets, the Raman spectrum of Pd/HNb₃O₈ nanosheets shows a significant weakening of all Raman modes, indicating that the crystallinity markedly decreases inside the microstructure of Pd-modified HNb₃O₈ nanosheets (Figure 1h). The Raman peaks of pristine HNb₃O₈ nanosheets at 1000–850 cm⁻¹, 700–500 cm⁻¹, 465 cm⁻¹, and 350–200 cm⁻¹ are the stretching modes of short Nb–O bond, long Nb–O bond, O–Nb–O linkage, and bending mode of O–Nb–O linkage, respectively.³¹ Meanwhile, the bond at 147 cm⁻¹ is most likely due to the residual TMA⁺ cations in the material system.³²

To elucidate the different electronic states of the elements inside

the material system, Pd/HNb₃O₈ and HNb₃O₈ were compared using X-ray photoelectron spectroscopy (XPS). The survey spectra of Pd/HNb₃O₈ and HNb₃O₈ (Figure S4, ESI†) present detailed element compositions on the nanosheets surface. The Pd 3d spectrum has two vivid peaks of Pd 3d_{5/2} and Pd 3d_{3/2} at 335.7 eV and 341 eV, respectively (Figure S4b, ESI†). The Nb 3d spectrum of Pd/HNb₃O₈ nanosheets displays two typical peaks of Nb⁵⁺ (3d_{5/2}) and Nb⁵⁺ (3d_{3/2}) at 207 eV and 209.6 eV along with two other peaks of Nb⁴⁺ (3d_{5/2}) and Nb⁴⁺ (3d_{3/2}) at 205.3 eV and 208 eV, respectively (Figure 1i). The two Nb⁴⁺ peaks in Pd/HNb₃O₈ show much stronger intensities than that in HNb₃O₈ (Figure S4d, ESI†), which is consistent with the higher atomic ratio of Nb⁴⁺ in Pd/HNb₃O₈. This suggests that the HNb₃O₈ nanosheets are reduced after the photoreduction process in an ambient environment. Furthermore, both pristine HNb₃O₈ (Figure S4e, ESI†) and Pd/HNb₃O₈ (Figure 1j) display two O 1s peaks at 531.7 eV and 530.1 eV, which belong to the lattice oxygen and oxygen bonded with Nb⁴⁺, respectively.^{28, 31}

Compared with pristine HNb₃O₈, the total atomic ratio of oxygen in Pd/HNb₃O₈ is slightly reduced by 1.24%, indicating that the lattice contains some oxygen defects (Figure S4f, ESI†). Using this

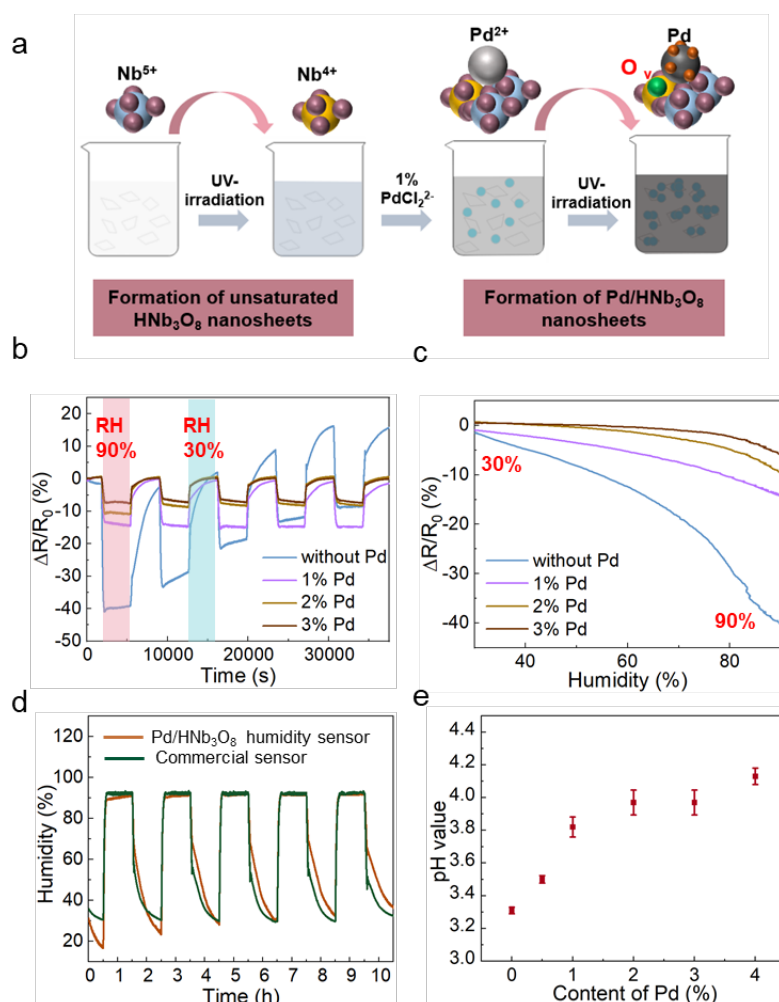


Figure 2. (a) Overview of the synthesis of 1% Pd/HNb₃O₈ nanosheets. (b) Cycle tests of HNb₃O₈ humidity sensors with different Pd contents and humidity variations from 30% to 90%. (c) Resistance change of different Pd contents of the Pd/HNb₃O₈ humidity sensor as a function of RH. (d) Long-time cycle tests of a 1% Pd/HNb₃O₈ humidity sensor compared with that of a commercial humidity sensor under the same RH. (e) pH results of the prepared HNb₃O₈ nanosheets solution with different Pd contents.

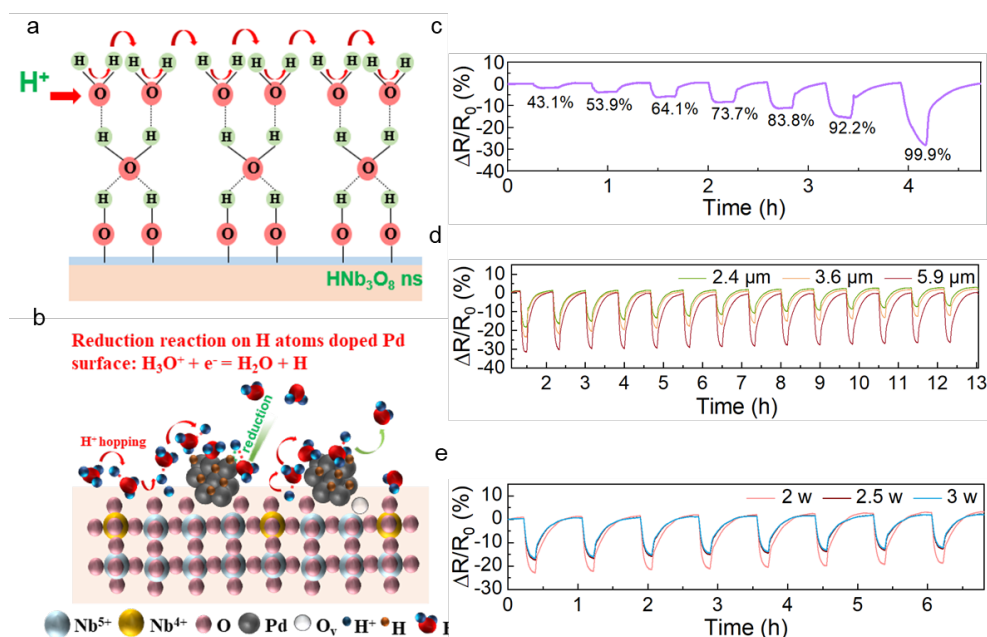


Figure 3. (a) Diagram of the humidity sensing mechanism of HNb_3O_8 nanosheets. (b) Schematic of the reduction reaction on H atoms assembled Pd/ HNb_3O_8 nanosheets surface under high RH. (c) Resistance change of 1% Pd/ HNb_3O_8 humidity sensor under different RHs. (d) Long-time cycle tests of different quantities of 1% Pd/ HNb_3O_8 nanosheets-based humidity under humidity variations from 30% to 95%. (e) Cycle measurements of 1% Pd/ HNb_3O_8 humidity sensors with different LIG electrodes produced at various laser powers.

Pd/ HNb_3O_8 material, a flexible humidity sensor designed for wearable applications is demonstrated by integrating with a microcontroller and wireless system (Figure 1k).

To study the humidity effect on the electrical behavior with different Pd contents in HNb_3O_8 , we measured the resistance in an oven where both the humidity and temperature could be controlled. The temperature was kept at 25 °C and RH was varied from 30% to 90%. The different contents of Pd-doped HNb_3O_8 nanosheets were synthesized using the same procedure as that to prepare 1% Pd/ HNb_3O_8 nanosheets beside the content of Pd precursor. (Figure 2a). The cycle tests of humidity sensors with different contents of Pd were conducted at a voltage bias of 5 V. Figure 2b shows the different moisture sensing behaviors of pristine HNb_3O_8 nanosheets and HNb_3O_8 nanosheets with a Pd content of 1%, 2%, and 3% (Figure S5, ESI†). To achieve a reliable humidity sensor capable of withstanding high humidity conditions for a long time, the response of each humidity sensor under a high humidity (90%) for 1 h was recorded repeatedly. The pristine HNb_3O_8 humidity sensor shows a highest resistance change of 40% under the humidity variation from 30% RH to 90% RH (Figure 2b). This is because the mild acidic HNb_3O_8 nanosheets system has a high affinity for water molecules.³³ Furthermore, this humidity sensor supports a high intensity of proton hopping in the physically absorbed water molecules when it is placed in a high humidity environment. Nonetheless, subjecting the pristine HNb_3O_8 humidity sensor to three cycles of humidity changes decreases the resistance change to only 22%. Additionally, the resistance change continuously fluctuates in the final two cycle tests, indicating the poor reproducibility and stability of pristine HNb_3O_8 humidity sensor. This is because the accumulation of hydroniums on nanosheets surface blocks the further proton hopping processes between protons and water molecules. On the other hand, although the 1% Pd/ HNb_3O_8 humidity sensor shows a relatively low resistance

change of 15%, it is quite stable even under 5 cycles of tests. Upon increasing the content of Pd to 2% and 3%, the humidity sensors display good stability, but their sensitivities are slightly reduced (Figure 2c). Among these four humidity sensors, the 1% Pd/ HNb_3O_8 nanosheet-based humidity sensor shows a superior humidity sensing performance in a prolonged stability test under a high humidity level (90%). To further validate the stable performance of the 1% Pd/ HNb_3O_8 humidity sensor, we used a commercial humidity sensor as the control under the same humidity variation conditions (Figure 2d). As expected, the sensing result of our humidity sensor almost matches that of the commercial humidity sensor, especially in the long detection period (1 h) and high humidity (90%). In addition to the reliable stability for long time of cyclic measurements, the 1% Pd/ HNb_3O_8 humidity sensor also shows a wide detection range from 30% RH to 99.9% RH (Figure S6, ESI†). To compare the modification effect of Pd with other metal nanoparticles, the humidity responses of Ag and Au nanoparticles-based humidity sensors were also investigated. As presented in Figure S7 (ESI†), both the Ag/ HNb_3O_8 and Au/ HNb_3O_8 nanosheets-based humidity sensors show very poor sensitivity and stability during the cycle test, suggesting that the Ag/Au nanoparticles are not suitable for improving the performance of HNb_3O_8 -based humidity sensors.

In principle, the stability of this humidity sensor is due to the effective regulation of proton-hopping in physically absorbed water molecules via the Pd-doped HNb_3O_8 nanosheets. As a type of acidic nanosheets, pristine HNb_3O_8 nanosheets possess a large amount of

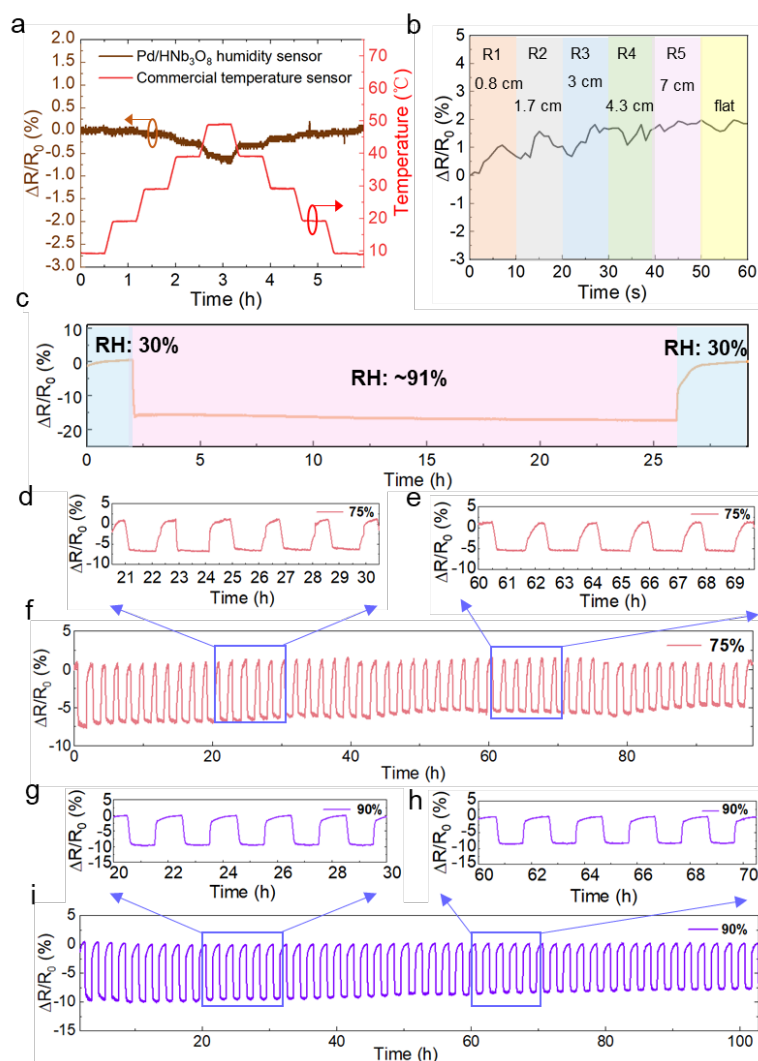


Figure 4. (a) Temperature dependent test of a 1% Pd/HNb₃O₈ humidity sensor under temperature variations from 10 °C to 50 °C. (b) Real-time bending result of a 1% Pd/HNb₃O₈ humidity sensor under various bending radii. (c) 24-h stability test of a 1% Pd/HNb₃O₈ humidity sensor under 90% RH. Long-time stability measurements (50 cycles) under (d)–(f) 75% RH and (g)–(i) 90% RH.

hydrogen ions. This is confirmed by the low pH value (3.31) of pristine HNb₃O₈ nanosheets solution. However, the cyclic measurement of this humidity sensor in Figure 2b displays performance degradations and upward fluctuations with the increasing of cyclic numbers, indicating the poor stability of pristine HNb₃O₈ nanosheets-based humidity sensor. This is due to that the accumulation of abundant hydroniums on the nanosheets surface restricts the further proton hopping process between protons and water molecules. For Pd/HNb₃O₈ nanosheets-based humidity sensors fabricated with 1%, 2%, and 3% of Pd, pH values are higher than pristine HNb₃O₈ nanosheets, which are 3.82, 3.97, and 3.97, respectively. This means a lower concentration of protons in Pd-modified nanosheets than that in pristine HNb₃O₈ nanosheets, leading to the decrease of sensitivity. However, the modification of Pd remarkably improved the stability of humidity sensors. The enhanced cyclic performance of Pd/HNb₃O₈ humidity sensor is attributed to the hydrogen atoms that are generated at the photoredox reaction, during which the hydrogen ions of HNb₃O₈ nanosheets are reduced to hydrogen. Then, the free hydrogen atoms are easily split and tightly

adsorbed on the surface of Pd nanoparticles due to the high dissociation ability of Pd. Hydrogen atoms are highly reductive, which are easy to reduce the unstable hydroniums (H₃O⁺) to water molecules, thereby enhancing the reproducibility of humidity sensor at cycle tests. Compared with HNb₃O₈ humidity sensor, the hydrogen atoms-enriched Pd/HNb₃O₈ humidity sensor owns an ability of regulating the excess hydroniums, which prevents the performance degradation caused by accumulation of hydroniums. Based on the sensitivity and stability, 1% Pd/HNb₃O₈ humidity sensor is used for further characterizations and demonstrations.

Similar to the sensing mechanism of most humidity sensors,^{4,34,35} water molecules from the outside first occupy the hydrophilic sites of vacancies in the HNb₃O₈ nanosheets due to double hydrogen bonds under a low humidity level. Then a second layer of water molecules is adsorbed on the first layer through hydrogen bonding. As the water molecules increase on the nanosheets surface, a high density of hydroniums is produced by the fraction of physically adsorbed water molecules under an applied field. The charge transfers between the hydroniums and water molecules, which is also called proton hopping,

is responsible for the reduced resistance of the HfNb_3O_8 humidity sensor (Figure 3a). This proton hopping process can be described as a Grotthuss chain reaction: $\text{H}_2\text{O} + \text{H}_3\text{O}^+ = \text{H}_3\text{O}^+ + \text{H}_2\text{O}$.^{13, 36, 37} The enhanced stability of the Pd/ HfNb_3O_8 humidity sensor is attributed to the high reactivity of H atoms on the Pd surface, which can easily reduce the surrounding hydroniums to water molecules, especially under a high humidity (Figure 3b).³⁸ Therefore, the concentration of hydroniums in proton hopping process reaches a balance at a certain RH. However, for the pristine HfNb_3O_8 nanosheets, although the sensitivity is higher, the accumulation of hydroniums at high humidity leads to an apparent performance degradation.

The Pd/ HfNb_3O_8 humidity sensor was further evaluated under different RHs. Although the resistance change of this humidity sensor is not linear, the resistance change difference is still clearly captured at different series of RH. When the humidity is above 85%, this humidity sensor shows an enhanced increment in resistance change, indicating the penetration of abundant water molecules into the inner layer of Pd/ HfNb_3O_8 nanosheets. (Figure 3c). To further optimize the humidity sensing behavior, we examined different quantities of nanosheets in the humidity sensors. The sensor formed by a 5.9 μm -thick Pd/ HfNb_3O_8 nanosheets shows a resistance change of 31% under a humidity level of around 95% RH. This is much higher than the results of 2.4 μm -thick (18%) and 3.6 μm -thick (23%) Pd/ HfNb_3O_8 nanosheets-based humidity sensors. However, this humidity sensor with relatively thick sensing material shows a relatively slower recover process, during which the resistance change fails to go back to original value (Figure 3d and Figure S8, ESI[†]). Generally, the middle thickness (3.6 μm) of Pd/ HfNb_3O_8 nanosheets-based humidity sensor is more reliable due to its relatively good sensitivity and repeatability at high humidity levels.

In addition, the LIG electrodes generated at different laser powers have a slight effect on the humidity sensing performance

(Figure 3e). The humidity sensors with LIG electrodes produced by 2.5 W and 3 W of laser power exhibit a faster response for water desorption than that produced by 2 W. This is because a high laser power realizes a LIG electrode with a higher porosity and a higher porosity with highly exposed surface area enhances the diffusion rate of electrons.^{39,40} The intensive porosity of LIG electrodes produced at different laser powers is verified by cross-sectional SEM images (Figure S9, ESI[†]). In general, silver or other metal electrodes are a better choice than porous graphene electrodes due to their high conductivity and stability. For humidity sensors, electrodes must maintain a very stable electrical performance in a long-time high-humidity environment. However, silver electrodes are unstable under high humidity conditions. In contrast, porous LIG electrodes maintain a quite stable performance (<1 %) even under 90% RH (Figure S10, ESI[†]), which is in good agreement with another report⁹. It should be noted that the resistance value of LIG is much smaller ($\sim 78 \Omega$) than that of Pd/ HfNb_3O_8 humidity sensor material ($> 1 \text{ M}\Omega$), resulting in that this small resistance change of LIG does not affect the output results of the sensor. Because LIG electrodes do not show a response to humidity, the humidity response of the humidity sensor shown in Figure 3 is due solely to the Pd/ HfNb_3O_8 nanosheets.

Next, we evaluated the impact of temperature and mechanical bending on the humidity sensor. A commercial temperature sensor was parallelly measured in a humidity and temperature controllable oven. The resistance change of the Pd/ HfNb_3O_8 humidity sensor is negligible under temperature variations from 10 $^\circ\text{C}$ to 40 $^\circ\text{C}$ while a slight decrease by around 0.5% is observed at the higher temperature range (40 $^\circ\text{C}$ – 50 $^\circ\text{C}$) due to the thermal-induced electron transfer. (Figure 4a). Furthermore, a real-time bending test of the Pd/ HfNb_3O_8 humidity sensor shows small variations under different bending radii (< 2 % in a bending radius of 0.8 cm) due to the wrinkled surface structure and good mechanical stability of Pd/ HfNb_3O_8 nanosheets

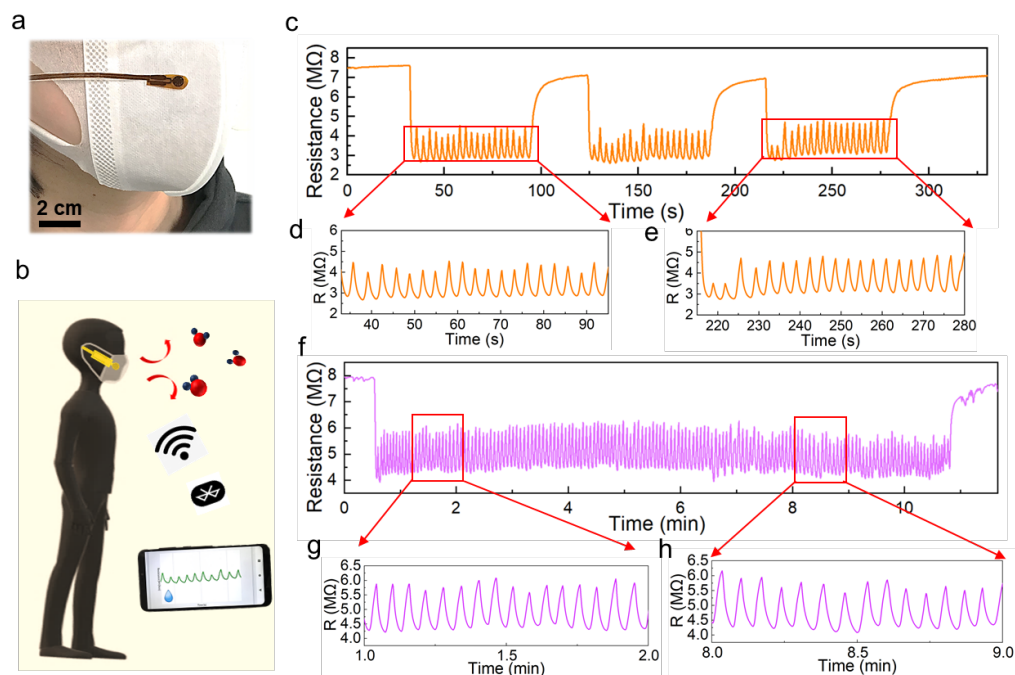


Figure 5. (a) Photo of a pint-sized device on a surgical mask worn on the subject's face. (b) Schematic of wireless respiration monitoring. (c)–(e) Respiratory rate of an adult in a calm state. (f)–(h) Long-time breathing test of a healthy adult in a calm state.

(Figure 4b). To understand the mechanism for the stability of temperature and mechanical bending, further detailed studies are required in the future, which is out of scope in this study. However, this small change is negligible to detect humidity level under mechanical bending due to much higher resistance change under humidity change.

To ensure the perdurability of the Pd/HNb₃O₈ humidity sensor in practical applications, a long-time stability test (24 h) at 90% RH and cycle tests with a long duration of stay (1 h) at 75% RH and 90% RH were performed. The humidity sensor shows a superior stability upon exposure to a high humidity level of RH 91% for 24 h (Figure 4c). This result demonstrates that the Pd/HNb₃O₈ humidity sensor balances charge transfer through the adsorbed water molecules. More importantly, the 50 cycles tests between 30% and 75% RH reveal the high reproducibility of the Pd/HNb₃O₈ humidity sensor (Figure 4d–f). The cycled curves under the same RH are consistent. Such a highly stable cycling behavior is also observed even at 90% RH for more than 100 h as only small degradations are captured after several repeated tests (Figure 4g–i). To further validate the reproducibility of this humidity sensor, another 273-cycle measurement was conducted. In comparison with the cyclic performance of commercial humidity sensor, Pd/HNb₃O₈ humidity sensor shows similar response for humidity variation from 50% to 90%, although small drifts can be observed after long-time measurements (Figure S11, ESI†).

Using the optimized humidity sensor, two applications were demonstrated. Human respiration monitoring, which is one of the most popular applications for human health care,^{15, 41–43} has gained much attention. First, we attached a humidity sensor on a surgical

mask worn on the face of an adult (Figure 5a). This pint-sized device followed a similar fabrication process, except it is covered by a porous humidity pass filter, which blocks the penetration of liquid water. Note that the humidity sensor with the filter shows a similar cycling performance as that without the membrane (Figure S12, ESI†). The sensor was connected to a microprocessor and wireless system to monitor real-time breathing (Figure 5b, S13, and S14, ESI†). The breathing test of a subject shows a highly repeated resistance change from 7 MΩ to 2.8 MΩ in the three measurement periods. Although the humidity response does not return to the initial resistance value while breathing, the peak-to-peak intervals are sufficiently distinct for identification (Figure 5c–e). Furthermore, the long-time respiration monitoring result confirms the high stability and repeatability of the Pd/HNb₃O₈ humidity sensor (Figure 5f–h). The measured respiration rate of this subject is about 15 times/min, which agrees with the respiration frequency of a healthy adult (12–20 times/min).

Additionally, the response and recovery time are two vital parameters to evaluate the response speed of a humidity sensor. The fabricated Pd/HNb₃O₈ humidity sensor shows a very fast response (~0.2 s) as the humidity level varies from 30% to 96% under a short breathing test, in which the humidity level was calibrated by a commercial sensor. This outstanding response speed is attributed to the large quantity of hydrophilic groups (Nb₂O₆) inside the nanosheets system. However, the high affinity with water molecules induces a side effect on the desorption process. To recover the original dry condition, ~3 s is required for the humidity sensor, denoting the relatively slow desorption speed of water molecules (Figure S15, ESI†).

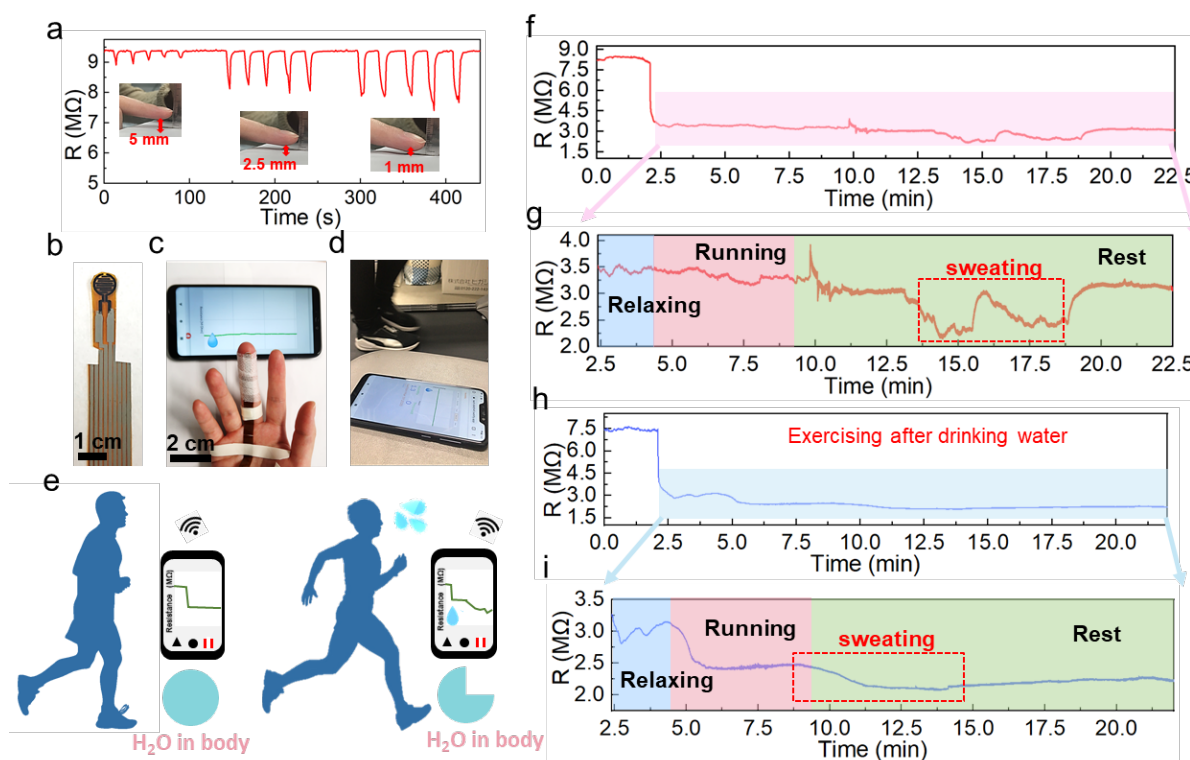


Figure 6. (a) Finger moisture detection under different gap distances. (b) Photo of the finger moisture application. (c)–(d) Photos of wireless finger moisture monitoring of a subject while running. (e) Schematics of finger moisture monitoring while exercising. Real-time finger moisture measurement of a subject conducted while running in a (f)–(g) dehydrate state and (h)–(i) well-hydrated state.

Another potential application is to monitor the sweat evaporation from the fingertips while exercising. Recently, fingertip moisture has been investigated utilizing different kinds of humidity sensors.^{12, 14, 44} Similarly, this Pd/HNb₃O₈ humidity sensor presents a fast response for non-contact moisture detection with different gap distances of 1 mm, 2.5 mm, and 5 mm between a fingertip and device (Figure 6a). To further show the reusability of this humidity sensor, the non-contact detection was successfully repeated even after 3 months (Figure S16, ESI†). Utilizing the high sensing performance to measure finger skin moisture, we investigated an additional application. Human skin can regulate the body temperature via heat loss from pores, which is always accompanied by sweating.^{45, 46} Normally, a healthy adult perspires after long-time exercise due to a rise in the body temperature.^{47, 48} Finger skin, which is a small part of human skin, plays a significant role in balancing body temperature and moisture. Here, we analyzed water loss, which corresponds to sweating during exercise, by wireless real-time monitoring of finger moisture (Figure 6b–c). The experiment involved a subject running on a treadmill at a speed of 8 km/h (Figure 6d). Fingers release moisture to keep the body temperature at a consistent value. The moisture level barely changes upon exercising, indicating mild and stable evaporation of water from the skin (Figure 6e). However, after a period of exercise, the skin moisture starts to increase due to dissipating the excess heat. To confirm this, the real-time finger moisture was monitored. Initially, the Pd/HNb₃O₈ humidity sensor was isolated from the finger skin by inserting a plastic sheet. Sensors with and without finger moisture interactions are stable under bending (Figure S17, ESI†).

The water loss process of this adult during exercise was recorded at two different states of body water content. One is the dehydrated state (Supporting movie), which means the subject exercised without drinking water 8 h prior to exercising. The finger moisture was measured after 2.5 min and was followed by 1.5 min of relaxation under calm conditions. During the relaxation period, the device resistance decreased from 8 MΩ to 3.5 MΩ, indicating a high moisture level surrounding the finger skin in the initial state (Figure 6f). It is worth noting that the finger moisture presents a very small change when the subject ran for 5 min in the dehydration state (Figure 6g). Interestingly, the humidity sensor clearly shows twice the resistance decrease after several minutes of rest. This suggests that the skin tends to maintain the water content in the body and releases the moisture when necessary to decrease the body temperature. Note that the initial value of resistance is eventually restored, verifying a high dehydration condition of body. In contrast, the monitoring result of the subject who drank sufficient water (500 mL) before the measurement shows a completely different resistance behavior (Figure 6h–i). An obvious reduction in the resistance by 0.6 MΩ is captured while running. When the subject stopped running, the resistance dropped to about 2.05 MΩ, denoting a sufficient water content in the body. Notably, the well-hydrated subject started sweating toward the end of the running process, whereas the subject under dehydration condition only began to sweat after a long resting time. This suggests that the skin spontaneously reduces water loss when the body is dehydrated. To summarize, the Pd/HNb₃O₈ humidity sensor opens a new path for dehydration diagnosis via real-time monitoring of finger moisture. However, further studies such as tests with a large number of groups are necessary before applying the proposed sensor to diagnose

dehydration.

Conclusions

We developed a flexible wireless humidity sensor to evaluate the dehydration state of a healthy adult and for other wearable applications using a stacked Pd/HNb₃O₈ nanosheets layer as a sensing material. Notably, this Pd-doped HNb₃O₈ humidity sensor with a wide detection range (30–99.9% RH) presents a superior stability and reproducibility during more than 100 h of cycle tests at 90% RH. The obtained steady performance over such long periods is due to the contributions of highly reductive H atoms dissociated on the Pd surface. Additionally, this humidity sensor can achieve a fast response time (0.2 s) and recovery time (3 s) under a short breath test. The response results of Pd/HNb₃O₈ humidity sensor are comparable with other material-based humidity sensors, especially at long-time cycle tests (Table S1, ESI†). This surface modification method for hydronium management in the humidity sensing process can be extended to other nanomaterial-based humidity sensors. Moreover, this commendable humidity sensor enables two vital applications for human health monitoring (*i.e.*, respiration detection on a surgical mask and moisture evaporation on the fingertip). The breathing test can precisely record the respiratory rate (15 times/min) of a healthy adult, which is a very important parameter to evaluate the health status. Furthermore, this proposed humidity sensor can be miniaturized into a finger-shaped size and attached on the finger skin to continuously monitor the moisture variations under different physiological states. The dehydration condition is successfully captured when the water content is insufficient in the human body while exercising. This affords a facile path for body dehydration diagnosis via real-time moisture detection. Considering the practical use in future wearable applications, it is better to integrate the devices into gloves or other wearable clothes, which is more convenient and comfortable for users.

Experimental Section

Synthesis of HNb₃O₈ nanosheets: The HNb₃O₈ nanosheets were synthesized using a reported cation intercalation stripping method.²⁹ First, a stoichiometric ratio of niobium oxide (Nb₂O₅, Sigma-Aldrich, 99.99%) and potassium carbonate (K₂CO₃, Tokyo Chemical Industry, >99%) were mixed and ground for about 45 min. The mixture was then dispersed in 20 mL ethanol for over 8 h and dried at 70 °C for overnight. Then the mixed powder was sintered at 900 °C for 10 h to form bulk KNb₃O₈. Next bulk HNb₃O₈ was formed out via a proton-exchange process. The obtained bulk KNb₃O₈ was added in 6 mol·L⁻¹ nitric acid solution (HNO₃, Sigma-Aldrich, 70%) and stirred in an ambient environment for 6 days. The bulk HNb₃O₈ was thoroughly washed with distilled water until the pH was 6–7. Finally, exfoliation of bulk HNb₃O₈ was achieved by intercalation of tetrabutylammonium cations (TBAOH, Sigma-Aldrich) into layered HNb₃O₈ for over two weeks.

Synthesis of Pd/HNb₃O₈ nanosheets: Pd-doped HNb₃O₈ nanosheets were fabricated by an ultraviolet light reduction reaction. Initially, 27 mg of HNb₃O₈ nanosheets were uniformly dispersed in a mixture of distilled water and ethanol with a ratio of 1:1 (total volume: 16 mL). Then the dispersed HNb₃O₈ solution was purged with N₂ gas for 10

min and subjected to ultraviolet light irradiation ($\lambda=365$ nm) for 30 min to generate unsaturated HNb_3O_8 nanosheets, and the solution went from white to dusty blue. After reduced Nb^{4+} was sufficiently generated in the HNb_3O_8 nanosheets, $10 \text{ mg}\cdot\text{mL}^{-1}$ Na_2PdCl_4 solution (1 wt% of Pd, Sigma-Aldrich, 98%) was directly injected into the unsaturated HNb_3O_8 nanosheets solution followed by another 1 h of ultraviolet light irradiation. During this process, the solution gradually turned dark grey, signifying that reduced palladium-embedded HNb_3O_8 nanosheets were formed. Finally, the 1% Pd/ HNb_3O_8 nanosheets were successfully obtained after washing several times with distilled water.

Fabrication of Pd/ HNb_3O_8 humidity sensor: Figure S1 details the fabrication process. The humidity sensor was fabricated by a simple drop-casting method. First, the polyimide film (thickness: 50 μm) was cut and scanned by the CO_2 laser system (VLS2.30, UNIVERSAL Laser System) at a wavelength of 10.6 μm and scanning power of 2 W. The generated graphene interdigitated electrodes (total area: 14 mm \times 12 mm) on the polyimide were then slightly cleaned with N_2 gas blowing. Subsequently, 600 μL (3.6 μm -thick) of the prepared 1% Pd/ HNb_3O_8 nanosheet solution ($5 \text{ mg}\cdot\text{mL}^{-1}$) was deposited onto the electrodes and baked at 100 $^\circ\text{C}$ for about 40 min. Finally, silver electrodes were screen-printed on the top of the graphene electrodes and baked at 70 $^\circ\text{C}$ for about 30 min. In addition, the top of the humidity sensor was covered with a porous humidity pass filter (TEMISH, Nitto Denko) to prevent direct contact between liquid water and the humidity sensor. At the same time, the silver electrodes were covered by a PET film to prevent them from oxidation when the device was attached on the finger.

Characterization: SEM characterization, including EDX mapping spectra, was conducted by a Hitachi S-4300 SEM. High-resolution images of Pd/ HNb_3O_8 nanosheets were characterized by a TEM (JEOL, JEM f200). XPS analysis was carried out using a ULVAC-PHI PHI 5000 Versaprobe II spectrometer with an Al $K\alpha$ (1486.6 eV) x-ray source. Raman spectra was measured using a commercial Raman spectrometer (HORIBA Raman, Labram HR Evolution). The film thickness of Pd/ HNb_3O_8 nanosheets was measured by a surface profile meter (Alpha-Step 500, KLA-Tencor). The fundamental study of the humidity sensor was conducted by placing it in a bench-top environment oven (Espec, SH-222) with variable temperatures and humidities. The temperature and relative humidity in the bench-top oven were calibrated by a commercial temperature sensor and humidity sensor. All data were collected by connecting the humidity sensor with a multi-channel data-logger (Hioki, LR8400). To perform the bending tests, the humidity sensor was attached on different radii of curved objects. Wireless monitoring of human breath and finger gas was conducted by connecting the humidity sensor with a small printed circuit board, which was charged by a portable lithium ion battery (3.7 V, 150 mAh). Data of wireless monitoring applications were synchronously collected by a smartphone capable of receiving wireless signals. To investigate the moisture evaporation from the finger skin under different physiological states, a treadmill (IGNIO, shock absorbing system) was utilized to conduct the experiments while exercising. The experiments to attach the sensors on skin were performed in compliance with the protocol approved by Osaka Prefecture University. Informed consents from all volunteers were

obtained for conducting physiological measurement and recording skin humidity.

Author contributions

Y. Lu and K. Takei conceived the project and designed the experiments. Y. Lu, K. Xu, and S. Honda conducted the sensor fabrication and characterizations. Y. Fujita developed the wireless system. S.-Y. Tang, T.-Y. Yang, and Y.-L. Chueh conducted XPS and TEM characterizations. All authors contributed to analyzing the data. Y. Lu, K. Xu, and K. Takei wrote the paper and all authors provide feedback.

Conflicts of interest

Y. L. and K. T. are inventors of a patent filed for the humidity sensor.

Acknowledgements

This work was supported by JST PRESTO (JPMJPR17J5), JSPS KAKENHI grants (JP17H04926 and JP18H05472), and the TEPCO Memorial Foundation. K. Xu was supported by JSPS International Research Fellowship. The authors greatly acknowledge for Shohei Fujio's help on SEM-EDX characterization.

Notes and references

1. P. Wang, M. Hu, H. Wang, Z. Chen, Y. Feng, J. Wang, W. Ling and Y. Huang, *Adv. Sci.*, 2020, **7**, 2001116.
2. K. Xu, Y. Lu, T. Yamaguchi, T. Arie, S. Akita and K. Takei, *ACS Nano*, 2019, **13**, 14348-14356.
3. H. Tai, Z. Duan, Y. Wang, S. Wang and Y. Jiang, *ACS Appl. Mater. Interfaces*, 2020, **12**, 31037-31053.
4. J. Yang, R. Shi, Z. Lou, R. Chai, K. Jiang and G. Shen, *Small*, 2019, **18**, 190280.
5. J. Wu, Y. M. Sun, Z. Wu, X. Li, N. Wang, K. Tao and G. P. Wang, *ACS Appl. Mater. Interfaces*, 2019, **11**, 4242-4251.
6. Y. Wang, L. Zhang, J. Zhou and A. Lu, *ACS Appl. Mater. Interfaces*, 2020, **12**, 7631-7638.
7. Y. Pang, J. Jian, T. Tu, Z. Yang, J. Ling, Y. Li, X. Wang, Y. Qiao, H. Tian, Y. Yang and T. L. Ren, *Biosens. Bioelectron.*, 2018, **116**, 123-129.
8. S. J. Choi, H. Yu, J. S. Jang, M. H. Kim, S. J. Kim, H. S. Jeong and I. D. Kim, *Small*, 2018, **14**, 1703934.
9. Y. Lu, K. Xu, L. Zhang, M. Deguchi, H. Shishido, T. Arie, R. Pan, A. Hayashi, L. Shen, S. Akita and K. Takei, *ACS Nano*, 2020, **14**, 10966-10975.
10. J. M. Nassar, S. M. Khan, D. R. Villalva, M. M. Nour, A. S. Almuslem and M. M. Hussain, *npj Flexible Electron.*, 2018, **2**, 24.
11. J. P. Giraldo, H. Wu, G. M. Newkirk and S. Kruss, *Nat. Nanotechnol.*, 2019, **14**, 541-553.
12. J. Peng, L. Peng, C. Wu, X. Sun, S. Hu, C. Lin, J. Dai, J. Yang and Y. Xie, *Adv. Mater.*, 2012, **24**, 1969-1974.
13. P. He, J. R. Brent, H. Ding, J. Yang, D. J. Lewis, P. O'Brien and B. Derby, *Nanoscale*, 2018, **10**, 5599-5606.
14. N. Li, Y. Jiang, C. Zhou, Y. Xiao, B. Meng, Z. Wang, D. Huang, C. Xing and Z. Peng, *ACS Appl. Mater. Interfaces*, 2019, **11**, 38116-38125.

15. L. Ma, R. Wu, A. Patil, S. Zhu, Z. Meng, H. Meng, C. Hou, Y. Zhang, Q. Liu, R. Yu, J. Wang, N. Lin and X. Y. Liu, *Adv. Funct. Mater.*, 2019, **29**, 1904549.
16. D. Rabus, J. M. Friedt, L. Arapan, S. Lamare, M. Baque, G. Audouin and F. Cherioux, *ACS Sens.*, 2020, **5**, 1075-1081.
17. J. Dai, H. Zhao, X. Lin, S. Liu, T. Fei and T. Zhang, *Adv. Electron. Mater.*, 2019, **6**, 1900846.
18. W. Xuan, X. He, J. Chen, W. Wang, X. Wang, Y. Xu, Z. Xu, Y. Q. Fu and J. K. Luo, *Nanoscale*, 2015, **7**, 7430-7436.
19. B. Stefano, W. Richard, W. Di, A. Michael, H. Samiul, S. Elisabetta, H. Nadine, K. Jani, R. Tapani, *ACS Nano*, 2013, **7**, 11166-11173.
20. J. Wu, Z. Wu, K. Tao, C. Liu, B.-r. Yang, X. Xie and X. Lu, *J. Mater. Chem. B*, 2019, **7**, 2063-2073.
21. Z. Yuan, H. Tai, Z. Ye, C. Liu, G. Xie, X. Du and Y. Jiang, *Sens. Actuators B Chem.*, 2016, **234**, 145-154.
22. X. Zhang, D. Maddipatla, A. Bose, S. Hajian, B. B. Narakathu, J. D. Williams, M. F. Mitchel and M. Z. Atashbar, *IEEE Sens. J.*, 2020, **20**, 12592-12601.
23. B. Cai, H. Yin, T. Huo, J. Ma, Z. Di, M. Li, N. Hu, Z. Yang, Y. Zhang and Y. Su, *J. Mater. Chem. C*, 2020, **8**, 3386-3394.
24. J. Zhao, N. Li, H. Yu, Z. Wei, M. Liao, P. Chen, S. Wang, D. Shi, Q. Sun and G. Zhang, *Adv. Mater.*, 2017, **29**, 1702076.
25. S.-L. Zhang, H.-H. Choi, H.-Y. Yue and W.-C. Yang, *Curr. Appl. Phys.*, 2014, **14**, 264-268.
26. D. Burman, S. Santra, P. Pramanik and P. K. Guha, *Nanotechnol.*, 2018, **29**, 115504.
27. A. S. Pawbake, R. G. Waykar, D. J. Late and S. R. Jadkar, *ACS Appl. Mater. Interfaces*, 2016, **8**, 3359-3365.
28. M.-Q. Yang, L. Shen, Y. Lu, S. W. Chee, X. Lu, X. Chi, Z. Chen, Q.-H. Xu, U. Mirsaidov, G. W. Ho, *Angew. Chem. Int. Ed*, 2019, **58**, 3077-3081.
29. L. Shen, Y. Xia, S. Lin, S. Liang and L. Wu, *Nanoscale*, 2017, **9**, 14654-14663.
30. Y. Zhao, X. Tan, W. Yang, C. Jia, X. Chen, W. Ren, S. C. Smith and C. Zhao, *Angew. Chem. Int. Ed*, 2020, **132**, 21677-21682.
31. J. Xiong, L. Wen, F. Jiang, Y. Liu, S. Liang and L. Wu, *J. Mater. Chem. A*, 2015, **3**, 20627-20632.
32. J. Chen, H. Wang, Z. Zhang, L. Han, Y. Zhang, F. Gong, K. Xie, L. Xu, W. Song and S. Wu, *J. Mater. Chem. A*, 2019, **7**, 5493-5503.
33. Y. T. Kang, C. C. Wang and C. Y. Chen, *J. Appl. Polym. Sci.*, 2020, **138**, 49729.
34. D. Zhang, X. Zong, Z. Wu and Y. Zhang, *Sens. Actuators B Chem.*, 2018, **266**, 52-62.
35. D. Zhang, X. Zong and Z. Wu, *Sens. Actuators B Chem.*, 2019, **287**, 398-407.
36. C. Lv, C. Hu, J. Luo, S. Liu, Y. Qiao, Z. Zhang, J. Song, Y. Shi, J. Cai and A. Watanabe, *Nanomaterials*, 2019, **9**, 422.
37. H. Farahani, R. Wagiran and M. N. Hamidon, *Sensors*, 2014, **14**, 7881-7939.
38. E. Pamaté Yambou, B. Gorska, P. Ratajczak and F. Béguin, *J. Mater. Chem. A*, 2020, **8**, 13548-13557.
39. K. Xu, Y. Lu, S. Honda, T. Arie, S. Akita and K. Takei, *J. Mater. Chem. C*, 2019, **7**, 9609-9617.
40. S. Wakabayashi, T. Arie, S. Akita and K. Takei, *ACS Omega*, 2020, **5**, 17721-17725.
41. K. Xu, Y. Lu and K. Takei, *Adv. Mater. Technol.*, 2019, **4**, 1800628.
42. S. Nakata, T. Arie, S. Akita and K. Takei, *ACS Sens.*, 2017, **2**, 443-448.
43. D. Yamamoto, S. Nakata, K. Kanao, T. Arie, S. Akita and K. Takei, *Adv. Mater. Technol.*, 2017, **2**, 1700057.
44. S. Kano, K. Kim and M. Fujii, *ACS Sens.*, 2017, **2**, 828-833.
45. Y. Yu, J. Nassar, C. Xu, J. Min, Y. Yang, A. Dai, R. Doshi, A. Huang, Y. Song, R. Gehlhar, A. D. Ames, W. Gao, *Sci. Robot.* 2020, **5**, eaaz7946.
46. Y. Yang, Y. Song, X. Bo, J. Min, O. S. Pak, L. Zhu, M. Wang, J. Tu, A. Kogan, H. Zhang, T. K. Hsiai, Z. Li and W. Gao, *Nat. Biotechnol.*, 2020, **38**, 217-224.
47. Y. Lin, M. Bariya, H. Y. Y. Nyein, L. Kivimäki, S. Uusitalo, E. Jansson, W. Ji, Z. Yuan, T. Happonen, C. Liedert, J. Hiltunen, Z. Fan and A. Javey, *Adv. Funct. Mater.*, 2019, **29**, 1902521.
48. M. Bariya, H. Y. Y. Nyein and A. Javey, *Nat. Electron.*, 2018, **1**, 160-171.